Journal for ImmunoTherapy of Cancer

PD-L1 directed bispecific Vδ2-T cell engager combines lysis of PD-L1 expressing tumor cells with PD-1 immune checkpoint inhibition and modulation of the tumor immune microenvironment

Lisa A King ,[1,2,3] Myrthe Veth,[1,2,3] Marieke Roos,[1,2,3] George L Scheffer,[1,2] Marko A Popovic,[4] Tanja D de Gruijl,[1,2,3] Hans J van der Vliet[1,2,5]

To cite: King LA, Veth M, Roos M, *et al*. PD-L1 directed bispecific Vδ2-T cell engager combines lysis of PD-L1 expressing tumor cells with PD-1 immune checkpoint inhibition and modulation of the tumor immune microenvironment. *Journal for ImmunoTherapy of Cancer* 2025;**13**:e012255. doi:10.1136/jitc-2025-012255

► Additional supplemental material is published online only. To view, please visit the journal online (https://doi.org/10.1136/jitc-2025-012255).

Accepted 08 October 2025

For numbered affiliations see end of article.

Correspondence to
Lisa A King;
l.king@amsterdamumc.nl

ABSTRACT

Background Despite the notable success of programmed death ligand 1 (PD-L1)/programmed death 1 (PD-1) immune checkpoint blockade in cancer, resistance remains a substantial challenge. Combining immune checkpoint blockade with direct targeting of effector T cells to tumor cells might improve outcome for a broader spectrum of patients with cancer. Phosphoantigen-responsive Vγ9Vδ2-T cells are potent immune cells that play a pivotal role in tumor immunosurveillance and can coordinate downstream immune activity. Here, we explored whether a Vδ2 bispecific T cell engager (bsTCE) directed against PD-L1 could combine lysis of PD-L1$^+$ tumor cells with PD-L1 immune checkpoint blockade.

Methods PD-L1 specific single domain antibodies (VHHs) were tested for binding to PD-L1 and their ability to interfere with PD-1 binding and function. One PD-L1 VHH was selected for fusion to a Vδ2-T cell receptor specific VHH (PD-L1xVδ2 bsTCE) and tested for its ability to activate Vγ9Vδ2-T cells and lyse melanoma cell lines, as well as patient-derived renal cell carcinoma (RCC) and metastatic melanoma cells. These patient-derived tumor suspensions were also used to explore effects on CD4$^+$ and CD8$^+$ T cells and myeloid cells. Infiltration of Vγ9Vδ2-T cells and tumor kill was tested in a three-dimensional tumor spheroid melanoma model.

Results A PD-L1xVδ2 bsTCE was generated and shown to block PD-1 binding resulting in the release of PD-1$^+$ cells from PD-L1 mediated inhibition. The PD-L1xVδ2 bsTCE also mediated robust Vγ9Vδ2-T cell activation, efficient lysis of RCC and melanoma cell lines and/or patient-derived tumor cells, and infiltration of Vγ9Vδ2-T cells into a three-dimensional melanoma spheroid model. Of interest, exposure of co-cultures of Vγ9Vδ2-T cells and patient-derived tumor suspensions to the PD-L1xVδ2 bsTCE resulted in upregulation of activation markers on tumor-infiltrated CD4$^+$ and CD8$^+$ T cells and lysis of PD-L1$^+$ myeloid cells with a shift in the myeloid compartment from macrophage-like cells to more mature dendritic cells with costimulatory molecule expression.

Conclusions A PD-L1xVδ2 bsTCE was generated that acts as PD-1/PD-L1 immune checkpoint inhibitor, enhances Vγ9Vδ2-T cell activation, infiltration and tumor lysis and reshapes the tumor microenvironment towards a more proinflammatory state. By targeting both PD-L1 expressing tumor and myeloid cells, it addresses key challenges of current therapies and thereby offers a promising novel therapeutic strategy.

WHAT IS ALREADY KNOWN ON THIS TOPIC

⇒ Immune checkpoint blockade targeting the programmed death ligand 1 (PD-L1)/programmed death 1 (PD-1) axis has transformed cancer immunotherapy. However, resistance, both primary and acquired, remains a significant challenge that limits the long-term efficacy of these therapies.

WHAT THIS STUDY ADDS

⇒ In an effort to overcome resistance, we have developed a novel bispecific T cell engager (bsTCE) that simultaneously targets PD-L1 and Vδ2-T cells. In this manuscript we report that this PD-L1xVδ2 bsTCE acts as a PD-1/PD-L1 immune checkpoint inhibitor, enhances Vγ9Vδ2-T cell activation, infiltration and tumor lysis and reshapes the tumor microenvironment towards a more proinflammatory state.

HOW THIS STUDY MIGHT AFFECT RESEARCH, PRACTICE OR POLICY

⇒ The PD-L1xVδ2 bsTCE allows for a multimodal approach to cancer immunotherapy by targeting both PD-L1 expressing tumor and myeloid cells. It therefore addresses key challenges of current therapies, and offers a promising novel therapeutic strategy.

INTRODUCTION

Immune response-modulating monoclonal antibodies (mAbs) represent one of the most promising strategies in cancer

immunotherapy, particularly through the demonstrated efficacy of immune checkpoint blockade.[1] Tumor cells and myeloid cells expressing programmed death ligand 1 (PD-L1) can suppress the immune response by inhibiting and inducing apoptosis of T cells expressing programmed death 1 (PD-1).[2] This mechanism has emerged as a key strategy by which tumors evade the host immune system.[2] In an expanding number of tumor indications, patients benefit from the use of approved mAbs that block the PD-L1/PD-1 axis. Responses can be durable, and are more common in patients with a high tumor mutation burden and associated higher frequency of neoantigens.[3] Despite these successes, many patients still do not benefit: some exhibit primary resistance, while others develop (acquired) resistance. This underscores the urgent need to refine existing approaches, rationally combine therapies or develop new strategies to achieve better outcomes for a broader range of patients.[4 5]

Combining immune checkpoint blockade with direct tumor cell lysis via bispecific antibody-mediated T-cell redirection presents a promising strategy to enhance antitumor activity. Previously, we demonstrated that Vδ2 bispecific T cell engagers (bsTCE) targeting tumor-associated antigens (TAA) can trigger Vγ9Vδ2-T cell activation, enabling the targeted lysis of (TAA-expressing) tumor cells.[6–10] Vγ9Vδ2-T cells, alongside $CD8^+$ T cells, are key players in tumor immunosurveillance. Their activation is mediated by phosphoantigens binding to butyrophilin (BTN) 3A1, which together with BTN2A1, triggers the T cell receptor (TCRs).[11 12] Vγ9Vδ2-T cells exhibit diverse antitumor functions, including direct tumor cell lysis through granzyme B, perforin, and Fas/FasL pathways, cytokine production (eg, interferon-gamma (IFNγ), tumor necrosis factor (TNF)), and antigen presentation to conventional T cells.[13–15] The ability of Vγ9Vδ2-T cells to drive broader immune activation through Vδ2 bsTCE-induced cytokine production and antigen presentation makes them particularly attractive for therapeutic applications.[9 10] Modulating the tumor microenvironment by activating antitumor immune effector cell populations while simultaneously targeting suppressive tumor cells and myeloid cells could further enhance efficacy. To this end, we set out to generate a Vδ2 bsTCE that would redirect Vγ9Vδ2-T cells to PD-L1 expressing tumor cells and myeloid cells and could simultaneously function as a PD-L1/PD-1 immune checkpoint inhibitor, thereby facilitating conventional T cell activation. By linking a high-affinity PD-L1 specific VHH with the ability to abrogate PD-L1/PD-1 interactions to a high affinity Vδ2-TCR specific VHH, a PD-L1xVδ2 bsTCE was generated that successfully redirected Vγ9Vδ2-T cell activity to both PD-L1 expressing tumor cells as well as PD-L1 expressing myeloid cells in patient-derived tumor samples. This resulted in Vγ9Vδ2-T cell activation, cytokine production and infiltration in a three-dimensional tumor spheroid model and tumor lysis in multiple in vitro and ex vivo models. Of interest, Vγ9Vδ2-T cell engagement by the PD-L1xVδ2 bsTCE was accompanied by modulation of the tumor immune microenvironment (TME) as evidenced by an increase in activation markers on tumor-infiltrated conventional $CD4^+$ and $CD8^+$ T cells as well as a shift in the myeloid compartment to higher rates of mature dendritic cells.

METHODS

Generation of PD-L1xVδ2 bsTCEs

The sequences of PD-L1-specific VHH clones 104D2, 104F5, and 104E12 were sourced from US Patent No. US-20160280786-A1. To generate PD-L1xVδ2 bsTCEs, these VHH clones were fused to the Vδ2-TCR specific VHH clone 5C8[16] using a Gly4Ser linker (VHH-G4S-VHH). Constructs were generated in both C-terminal and N-terminal orientations, resulting in the following bsTCEs: 104D2×5C8, 5C8×104D2, 104F5×5C8, 5C8×104F5, 104E12×5C8, and 5C8×104E12. Purified proteins were produced by ImmunoPrecise Antibodies using DNA-transfected HEK293E cells, rmp-Protein-A affinity chromatography and preparative size-exclusion chromatography.

Cell lines

HEK293T wild type (WT) cells were transfected to express PD-L1 using 50 µg pLX304 (HsCD00440445, DNASU) and 100 µg polyethylenimine (23966–1, Polysciences). PD-L1 expression was checked after 24 hours using flow cytometry and $PD\text{-}L1^+$ HEK293T cells were enriched using magnetic cell separation with antigen-presenting cell (APC)-labeled PD-L1 (clone MIH1, 17-5983-42, eBioscience) combined with anti-mouse IgG microbeads (130-048-402, Miltenyi Biotec). Melanoma cell lines BRO,[17] WM9[18] and MEL-AKR[19] were described previously and their identities were confirmed by short tandem repeat analysis, using the human cell line authentication service provided by Eurofins based on 21 independent PCR-single-locus-technology, following the ISO 17025 standard guidelines (https://www.eurofinsgenomics.eu/en/genotyping-gene-expression/applied-genomics-services/cell-line-authentication/). A375 was obtained from ATCC (CRL-1619). MEL-23 and MEL-25 were in-house generated from metastatic tumor samples collected from advanced-stage patients. These patients were enrolled under informed written consent in an institutional review board (IRB)-approved clinical study of autologous whole-cell vaccination at the VU University medical center between 1987 and 1998.[20] The collected tumor tissue was minced with a scalpel and dissociated three times for 45 min with 0.02% DNase I (Boehringer) and 0.14% collagenase (Boehringer) in Hanks' Balanced Salt Solution (Whittaker Bioproducts). The obtained cell suspensions were processed and cryopreserved within 24 hours of surgical removal.[21] After thawing single-cell suspensions were cultured until confluency after which non-adherent cells were removed.[22] Melanoma identity was confirmed by flow cytometry-based staining for melanoma-associated chondroitin sulfate proteoglycan.[22] Above-mentioned

tumor cell lines were maintained in Dulbecco's Modified Eagle's Medium (41 965–039, Gibco) supplemented with 10% (v/v) fetal calf serum (04-007-1A, Biological Industries), 0.05 mM β-mercaptoethanol (200-646-6, Merck), 100 IU/mL sodium penicillin, 100 µg/mL streptomycin sulfate and 2.0 mM L-glutamine (PSG, 10 378–016, Life Technologies). Vγ9Vδ2-T cells were isolated from healthy donor peripheral blood mononuclear cells (PBMCs), expanded as described before.[6] In short, Vγ9Vδ2-T cells were isolated from PBMC using magnetic bead sorting with fluorescein isothiocyanate (FITC)-labeled Vδ2 mAbs (online supplemental table S1) in combination with anti-mouse IgG microbeads (Miltenyi). Purified Vγ9Vδ2-T cells were stimulated weekly with irradiated feeder mix consisting of healthy donor PBMC (1×106 cells/mL), JY cells (1×105 cells/mL, 94022533, ECACC), interleukin (IL)-7 (10 U/mL, R&D Systems), IL-15 (10 ng/mL, eBioscience), and PHA (50 ng/mL, Thermo Fisher Scientific) and used in experiments if purity of Vγ9Vδ2-T cells was >95% of total cells. Dead feeder cells and debris were removed from Vγ9Vδ2-T cells by density gradient centrifugation using Lymphoprep (AXI-1114547, Fresenius) before using them in functional experiments. Cell lines were kept at 37°C in a humidified atmosphere containing 5% CO_2.

Flow cytometry

Cells were resuspended in phosphate-buffered saline (PBS) (1073508600, Fresenius Kabi) supplemented with 0.5% bovine serum albumin (M090001/03, Fisher Scientific) and 20 mg/mL NaN3 (247-852-1, Merck) and incubated with fluorochrome-labeled antibodies (Abs, online supplemental table S1) for 30 min at 4°C. Unbound fluorochrome-labeled Abs were washed away. The LSR Fortessa XL-20 (BD) was used for data acquisition and flow cytometry data were analyzed using Kaluza Analysis V.1.3 (Beckman Coulter) or FlowJo V.10.6.1 and 10.7.2 (Becton Dickinson). Cytometric bead array (CBA) data were analyzed with FCAP Array software V.3.0 (BD)

Target cell binding

Binding of PD-L1xVδ2 bsTCEs to PD-L1 and Vγ9Vδ2-T cells was determined by incubating HEK293T WT (control), HEK293T PD-L1$^+$ or expanded healthy donor-derived Vγ9Vδ2-T cells with a concentration range of the PD-L1xVδ2 bsTCE for 45 min at 4°C. Cells were extensively washed (5×) to remove unbound PD-L1xVδ2 bsTCE and binding was detected using FITC-labeled rabbit-anti-llama polyclonal antibody (BET A160-100F, Bioke) which was incubated for 30 min at 4°C. Unbound detection antibody was washed away and binding was analyzed using flow cytometry.

PD-1/PD-L1 blockade

Two assays were used to determine if the PD-L1xVδ2 bsTCE can block PD-1/PD-L1 interactions. Recombinant biotin-labeled PD-1 (10 µg/mL, 71 109–1, BPS Biosciences) was pre-incubated with HEK293T PD-L1$^+$ cells for 45 min at 4°C. Cells were washed and a concentration range of the PD-L1xVδ2 bsTCE was added and incubated for 45 min at 4°C. Cells were extensively washed (5×) to remove unbound PD-L1xVδ2 bsTCE and binding of the PD-1 protein was detected using APC-labeled streptavidin conjugate which was incubated for 30 min at 4°C. Unbound streptavidin conjugate was washed away and binding was analyzed using flow cytometry.

Second, the commercially available PD-1/PD-L1 blockade bioassay (J1250, Promega) was used. To do so, CHO-K1 cells (stably expressing PD-L1 and a cell surface protein designed to activate cognate TCRs in an antigen-independent manner) were thawed, and incubated for 24 hours at 37°C and 5% CO_2. Jurkat T cells (stably expressing human PD-1 and NFAT-induced luciferase) were thawed and co-cultured with CHO-K1 cells in the presence or absence of a concentration range of PD-L1xVδ2 bsTCE, nivolumab (Bristol Myers Squibb) or durvalumab (AstraZeneca BV) for 6 hour. Bio-Glo reagent was added and luminescence was measured using a luminescence plate reader (Glomax, Promega). The following calculation was used: relative light units (RLU) antibody – background / RLU no antibody control – background=-fold induction.

Vγ9Vδ2-T cell activation and tumor cell lysis

HEK293T WT (control), HEK293T PD-L1$^+$, BRO, WM9, MEL-AKR, A375, MEL-23 or MEL-25 were co-cultured for 24 hours with expanded healthy donor-derived Vγ9Vδ2-T cells (1:1 effector to target (E:T) ratio) in the presence or absence of 1 or 100 nM PD-L1xVδ2 bsTCE. PD-L1xVδ2 bsTCE-mediated Vγ9Vδ2-T cell activation was determined by assessing expression of CD107a (anti-CD107a mAb added at the start of culture), CD25 and 4-1BB. Tumor cytotoxicity was determined using a viability dye in combination with 123count eBeads counting beads (01-1234-42, Thermo Fisher Scientific).

Primary RCC and metastatic melanoma cultures

For functional experiments, patient-derived cryopreserved dissociated primary renal cell carcinoma (RCC) and metastatic melanoma single-cell suspensions (dissociation process described before[21]) were used. RCC and melanoma single-cell suspensions were thawed and cultured for 2 or 5 days with or without expanded healthy donor-derived Vγ9Vδ2-T cells and 10 µg/mL durvalumab, 100 nM PD-L1xVδ2 bsTCE or medium control. Expression of activation (CD25, 4-1BB) and degranulation (CD107a) markers and expression of PD-1 and TIM-3 on Vγ9Vδ2-T cells, CD4$^+$ T cells and CD8$^+$ T cells was determined after 2 days using fluorescently labeled antibodies and flow cytometry. Supernatants collected from these 2-day cultures were used to analyze IL-2, IL-4, IL-6, IL-10, IFNγ, TNF and IL-17A secretion through the human Th1/Th2/Th17 CBA kit (560484, BD). Phenotypic analysis of CD45$^+$HLA-DR$^+$CD11c$^+$ myeloid cells was done after 5 days using fluorescently labeled antibodies against CD80, CD83, CD86, CD14, CD163, BDCA-3 and

TIM-3 throughflow cytometry. Tumor cytotoxicity was determined after 2 and 5 days using 7AAD (A9400-1MG, Sigma) and 123counting eBeads (01-1234-42, Thermo Fisher) followed by flow cytometry analysis.

Spheroid cultures

In order to determine PD-L1xVδ2 bsTCE-mediated Vγ9Vδ2-T cell activation, tumor cell cytotoxicity and infiltration in a three-dimensional in vitro setting, BRO tumor cells were used to generate tumor spheroids. BRO tumor cells (5,000) were cultured overnight in nuclon sphere-treated 96-well plates (174925, Thermo Fisher Scientific) to generate spheroids. Expanded healthy donor-derived Vγ9Vδ2-T cells (6,000) were co-cultured with 1 BRO spheroid per condition for 24 hours in the presence or absence of 100 nM PD-L1xVδ2 bsTCE. Spheroid-infiltrated Vγ9Vδ2-T cells (termed IN fraction) were separated from non-infiltrated Vγ9Vδ2-T cells (termed OUT fraction) by washing twice with PBS and carefully removing the supernatant from the spheroids after they had sunk to the bottom. Fluorescently labeled antibodies against 4-1BB, CD25 and PD-1 were used for phenotypic analysis of Vγ9Vδ2-T cells. Cytotoxicity of BRO spheroids was determined by trypsinizing them to retrieve a single-cell suspension (also comprising the IN Vγ9Vδ2-T cell fraction). Cells were prepared and stained for flow cytometry analysis.

Vγ9Vδ2-T cell infiltration into BRO spheroids was visualized using confocal microscopy. To do so, Vγ9Vδ2-T cells were stained with a SPY555-DNA dye (1000×, SC201, Spirochrome) for 24 hours at 37°C while BRO tumor cells were stained with a SPY650-DNA dye (1000×, SC501, Spirochrome) during spheroid formation. Cells were washed, transferred to a high bioinert 8-well imaging µ-slide (80800, Ibidi) and co-cultured (1 BRO spheroid and 6,000 Vγ9Vδ2-T cells) in the presence or absence of 100 nM PD-L1xVδ2 bsTCE in the environmental chamber at 37°C and 5% CO_2 within the Nikon AXR LC for 8 hours. Each well was imaged every 20 min with 52 Z-stacks and a 10x objective. Images were analyzed with Imaris (Oxford Instruments), which was used to identify spheroids by using the "surface" tool, and Vγ9Vδ2-T cells by using the "spots" tool. The program calculated the shortest distance of each Vγ9Vδ2-T cell (spot) to the spheroid (surface). The sum of the negative values (Vγ9Vδ2-T cells within spheroid) was calculated per condition per time point to determine the amount of spheroid-infiltrating Vγ9Vδ2-T cells over time.

Statistical analysis

GraphPad Prism V.9.1.0 (GraphPad Software) was used for statistical analyses. Data were analyzed using paired t test or one-way analysis of variance with Dunnett multiple comparisons test. $p<0.05$ was considered significant and indicated with asterisks: *p<0.05, **p<0.01, ***p<0.001 and ****p<0.0001. EC50 values were calculated using non-linear regression analysis with GraphPad Software.

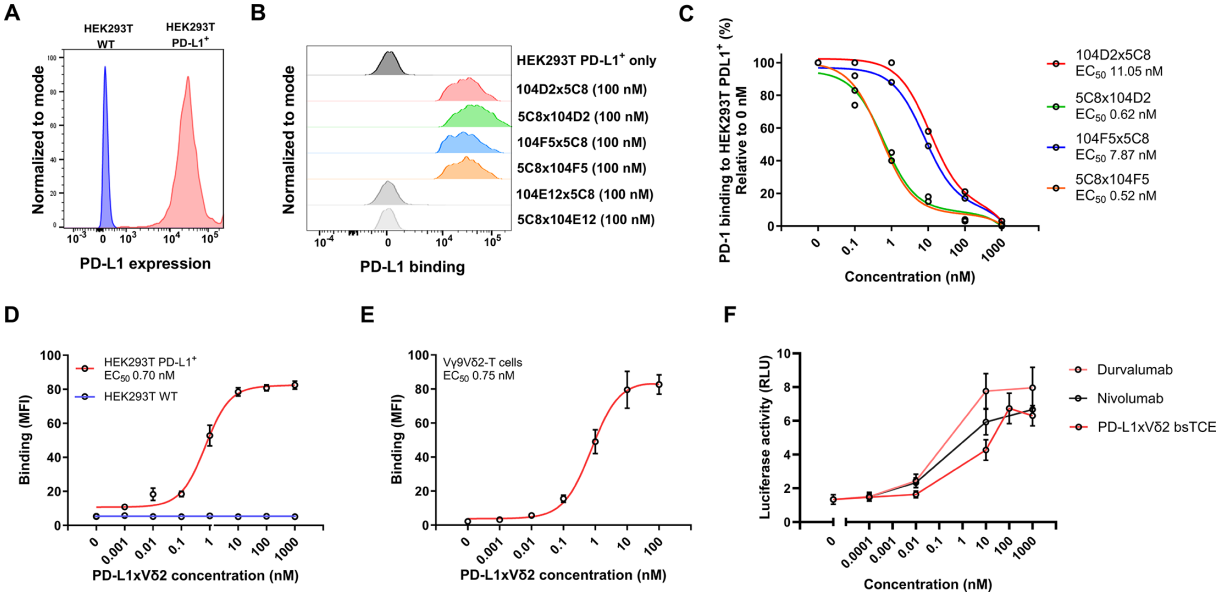

Figure 1 Binding of PD-L1xVδ2 bsTCEs to HEK293T PD-L1+ tumor cells and Vγ9Vδ2-T cells and their blocking capacity of PD-1/PD-L1 interactions. (A) PD-L1 expression on HEK293T WT and HEK293T PD-L1+ tumor cells shown in histogram. (B) Binding of six PD-L1xVδ2 bsTCEs (100 nM) to HEK293T PD-L1+ tumor cells (n=1/bsTCE) shown in histograms. (C) Binding of biotin-labeled recombinant PD-1 (10 µg/mL) to PD-L1+ HEK293T tumor cells±concentration range of four PD-L1xVδ2 bsTCEs (n=1/bsTCE). (D) PD-L1xVδ2 bsTCE (5C8-104D2) binding to HEK293T PD-L1+ tumor cells (n=3). (E) PD-L1xVδ2 bsTCE (5C8-104D2) binding to Vγ9Vδ2-T cells (n=3). (F) Luciferase activity as assessed after a 6-hour co-culture of PD-1+ Jurkat cells and PD-L1+ CHO cells±concentration range durvalumab, nivolumab or PD-L1xVδ2 bsTCE (5C8-104D2) (n=3). Data are generated throughflow cytometry (A–E) or through a luminescence plate reader (F). Data represent mean (B, C) or mean and SEM (D–F). bsTCE, bispecific T cell engager; PD-1, programmed death 1; PD-L1, programmed death ligand 1; WT, wild-type; MFI, mean fluorescence intensity; RLU, relative light units.

RESULTS

Generation of a PD-L1xVδ2 bsTCE that binds both PD-L1 and Vδ2 and blocks PD-1/PD-L1 interactions

Six PD-L1xVδ2 bsTCEs were generated by fusing PD-L1-specific VHH clones 104D2, 104F5, and 104E12 to the high-affinity Vδ2-TCR-specific VHH clone 5C8, using a Gly4Ser linker, in both N-terminal and C-terminal orientations. While PD-L1xVδ2 bsTCEs containing PD-L1 VHH clones 104D2 and 104F5 bound to PD-L1$^+$ HEK293T tumor cells, no binding was observed with the PD-L1xVδ2 bsTCEs incorporating clone 104E12 (figure 1A,B; figure 1A shows PD-L1 expression on PD-L1 transfected HEK239T cells compared with WT cells). The ability of the 104D2-VHH and 104F5-VHH containing PD-L1xVδ2 bsTCEs to inhibit PD-1/PD-L1 interactions was assessed by studying recombinant biotin-labeled PD-1 displacement from PD-L1$^+$ HEK293T tumor cells. As shown in figure 1C, increasing concentrations of both PD-L1xVδ2 bsTCEs resulted in a dose-dependent reduction of PD-1 binding. Displacement of PD-1 was most pronounced with C-terminal positioning of the PD-L1 VHHs (EC_{50} values: 5C8×104D2 0.62 nM and 5C8×104F5 0.52 nM vs 104D2×5C8 11.05 nM and 104F5×5C8 7.87 nM) with no notable difference between clones 104D2 and 104F5. Based on its higher binding intensity to PD-L1$^+$ HEK293T tumor cells, the 5C8×104D2 based bsTCE was selected for further experiments and from here on referred to as PD-L1xVδ2 bsTCE. This PD-L1xVδ2 bsTCE bound with high affinity (EC_{50} for binding 0.70 nM) to PD-L1$^+$ HEK293T cells and showed no binding to non-transfected HEK293T cells (figure 1D). The EC_{50} for binding to Vγ9Vδ2-T cells was 0.75 nM which is in line with our earlier observations for the Vδ2-specific VHH[9] (figure 1E). To evaluate whether the PD-L1xVδ2 bsTCE could also functionally block the interaction between PD-1 and PD-L1, a cell-based bioassay was used in which release of the PD-1/PD-L1 axis was tested in co-cultures of PD-1$^+$ Jurkat cells and PD-L1$^+$ CHO cells. As shown in figure 1F, the PD-L1xVδ2 bsTCE resulted in a dose-dependent abrogation of the PD-L1 mediated inhibition of PD-1$^+$ Jurkat cells, as reflected by an increase in luciferase activity. A similar effect was observed with the positive control antibodies in these assays (ie, the PD-L1 blocking mAb durvalumab and the PD-1 blocking mAb nivolumab).

Collectively, these data show that the generated PD-L1xVδ2 bsTCE mediates specific and high-affinity binding to PD-L1-expressing cells as well as Vγ9Vδ2-T cells and has the ability to block the interaction between PD-1 and PD-L1.

The PD-L1xVδ2 bsTCE triggers robust Vγ9Vδ2-T cell activation and lysis of PD-L1$^+$ tumor cells

We next explored the ability of the PD-L1xVδ2 bsTCE to induce Vγ9Vδ2-T cell activation and tumor cell lysis. In 24 hours co-cultures of Vγ9Vδ2-T cells and HEK293T WT or HEK293T PD-L1$^+$ tumor cells, Vγ9Vδ2-T cell degranulation and tumor cell lysis were only observed in co-cultures with PD-L1$^+$ tumor cells (figure 2A,B). No reactivity was observed using a control bsTCE (104E12×5C8). As these HEK293T PD-L1$^+$ tumor cells expressed high levels of PD-L1, we next explored the activity of the PD-L1xVδ2 bsTCE in co-cultures of Vγ9Vδ2-T cells and the patient-derived melanoma tumor cell lines BRO, WM9, AKR and A375 that express lower to substantially lower levels of PD-L1 (figure 2C). As shown in figure 2D,E, the PD-L1xVδ2 bsTCE triggered Vγ9Vδ2-T cell activation, as assessed by upregulation of the activation markers CD25 and 4-1BB and the degranulation marker CD107a, and subsequent tumor cell lysis of all of these tumor cell lines, despite PD-L1 expression being quite low in WM9 and AKR cell lines. It is known that IFNγ, which is secreted at high levels by activated Vγ9Vδ2-T cells,[9 10] can upregulate PD-L1 expression.[23] IFNγ induced PD-L1 upregulation on the melanoma tumor cell lines was confirmed, and may therefore have contributed to the observed potency of the PD-L1xVδ2 bsTCE against PD-L1^{low} melanoma tumor cells (figure 2F). The activity of the PD-L1xVδ2 bsTCE was also tested using low-passage melanoma cell lines (two to three passages) that were isolated in-house from lymph node metastases of two patients. Both of these patient-derived cell lines expressed PD-L1, which could be further increased by IFNγ (figure 2G,H). When Vγ9Vδ2-T cells were co-cultured with these low-passage melanoma cell lines, the PD-L1xVδ2 bsTCE triggered robust Vγ9Vδ2-T cell degranulation and tumor cell lysis (figure 2I).

In conclusion, the generated PD-L1xVδ2 bsTCE efficiently cross-links Vγ9Vδ2-T cells and PD-L1 expressing tumor cell lines (both established and low-passage patient-derived) to trigger Vγ9Vδ2-T cell activation and lysis of PD-L1$^+$ tumor cells.

PD-L1xVδ2 bsTCE triggers Vγ9Vδ2-T cell-mediated antitumor activity in co-cultures with patient-derived renal cell carcinoma and melanoma single-cell suspensions

Next we assessed whether the PD-L1xVδ2 bsTCE could also induce Vγ9Vδ2-T cell activation and tumor lysis in co-cultures of Vγ9Vδ2-T cells with patient-derived dissociated RCC and metastatic melanoma tumor samples, comprising the entire TME. The majority of tumor cells present in these samples was found to express PD-L1 (figure 3A). Vγ9Vδ2-T cells were added to tumor samples in a 1:10 E:T ratio as infiltrating Vγ9Vδ2-T cell frequencies were relatively low and variable between tumor suspensions (figure 3B). After a 2-day co-culture, Vγ9Vδ2-T cells expressed significantly higher levels of the activation markers CD25 and 4-1BB, the degranulation marker CD107a, and the immune checkpoint receptors PD-1 and TIM-3 (figure 3C). Upregulation of these markers was generally less pronounced when Vγ9Vδ2-T cells were exposed to melanoma as compared with RCC samples. Levels of these receptors on Vγ9Vδ2-T cells did not change in co-cultures containing the anti-PD-L1 mAb durvalumab rather than the PD-L1xVδ2 bsTCE (figure 3D). Consistent with the observed activation of Vγ9Vδ2-T cells in response to the PD-L1xVδ2 bsTCE, supernatants from the 2-day co-cultures showed significantly increased levels of IFNγ, TNF, and IL-2. There was a trend for higher levels of IL-4 in the PD-L1xVδ2 bsTCE

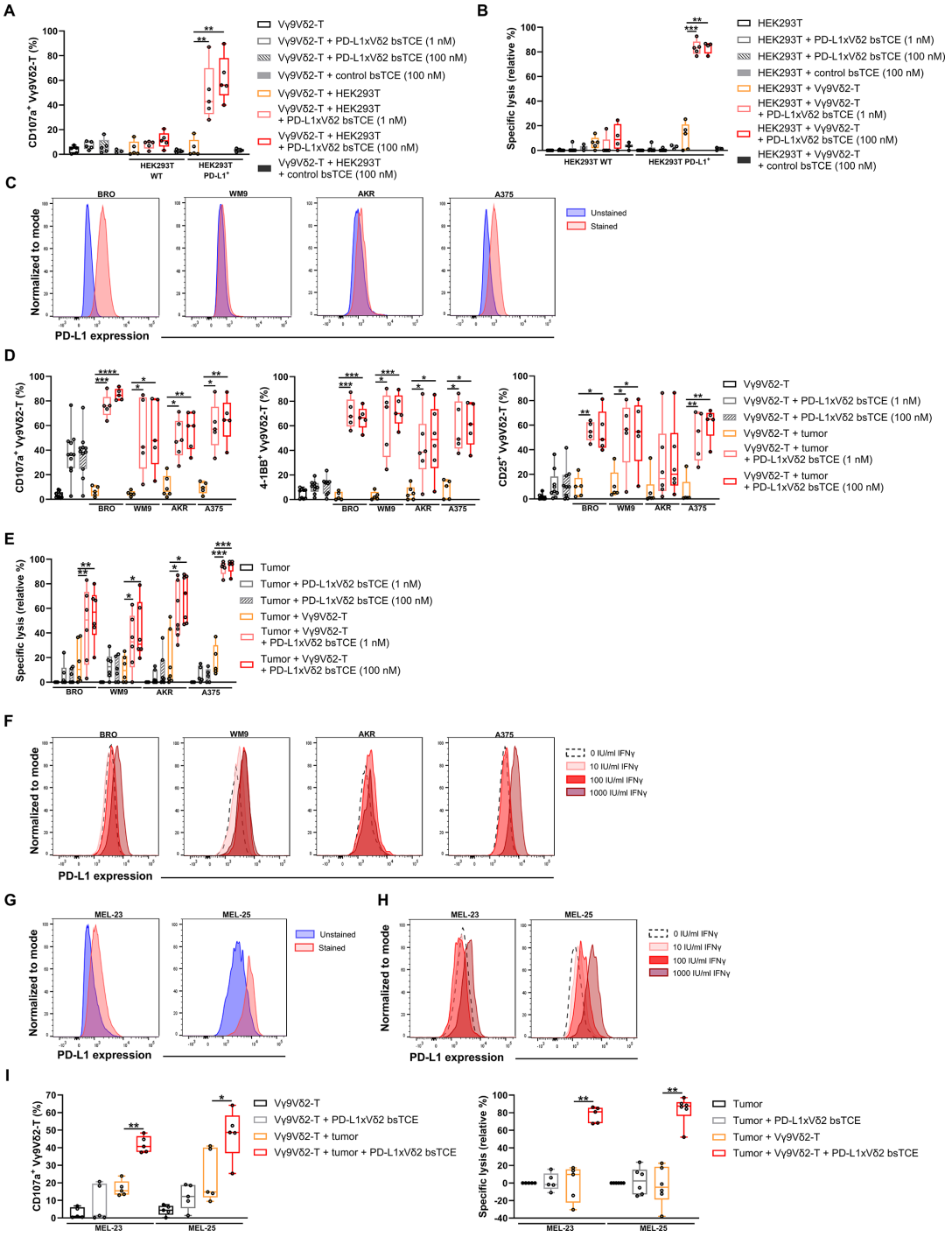

Figure 2 PD-L1xVδ2 bsTCE triggers Vγ9Vδ2-T cell activation and lysis of PD-L1-expressing tumor cells. (A–B) Expression of CD107a on Vγ9Vδ2-T cells (A, n=5) and lysis of HEK293T WT and HEK293T PD-L1$^+$ tumor cells (B, n=8) (1:1 E:T ratio) after 24 hours co-culture in the presence of 0, 1 or 100 nM PD-L1xVδ2 bsTCE or 100 nM control bsTCE (104E12×5C8). (C) PD-L1 surface expression levels on BRO, WM9, AKR and A375 shown in histograms. (D–E) Expression of CD107a, 4-1BB and CD25 on Vγ9Vδ2-T cells (D, n=5–6) and lysis of BRO, WM9, AKR and A375 tumor cells (E, n=6–7) (1:1 E:T ratio) after 24 hours co-culture in the presence of 0, 1 or 100 nM PD-L1xVδ2 bsTCE. (F) PD-L1 surface expression levels on BRO, WM9, AKR and A375 after overnight culture with 0, 10, 100 or 1,000 IU/mL IFNγ shown in histograms. (G) PD-L1 surface expression levels on low-passage lymph node metastasis-derived cell lines MEL-23 and MEL-25 shown in histograms. (H) PD-L1 surface expression levels on MEL-23 and MEL-25 after overnight culture with 0, 10, 100 or 1,000 IU/mL IFNγ shown in histograms. (I) Expression of CD107a on Vγ9Vδ2-T cells (I, n=5) and lysis of MEL-23 and MEL-25 tumor cells (J, n=5–6) (1:1 E:T ratio) after 24 hours co-culture in the presence of 0 or 100 nM PD-L1xVδ2 bsTCE. Data are all generated throughflow cytometry. Individual data points are indicated using open circles and box and whisker plots indicate the median, 25th to 75th percentiles and minimum to maximum. One-way ANOVA with Dunnett's multiple comparisons test was used (A, B, E, F, I), *p≤0.05, **p≤0.01, ***p≤0.001, ****p≤0.0001. ANOVA, analysis of variance; bsTCE, bispecific T cell engager; E:T, effector to target; IFNγ, interferon-gamma; PD-L1, programmed death ligand 1; WT, wild-type.

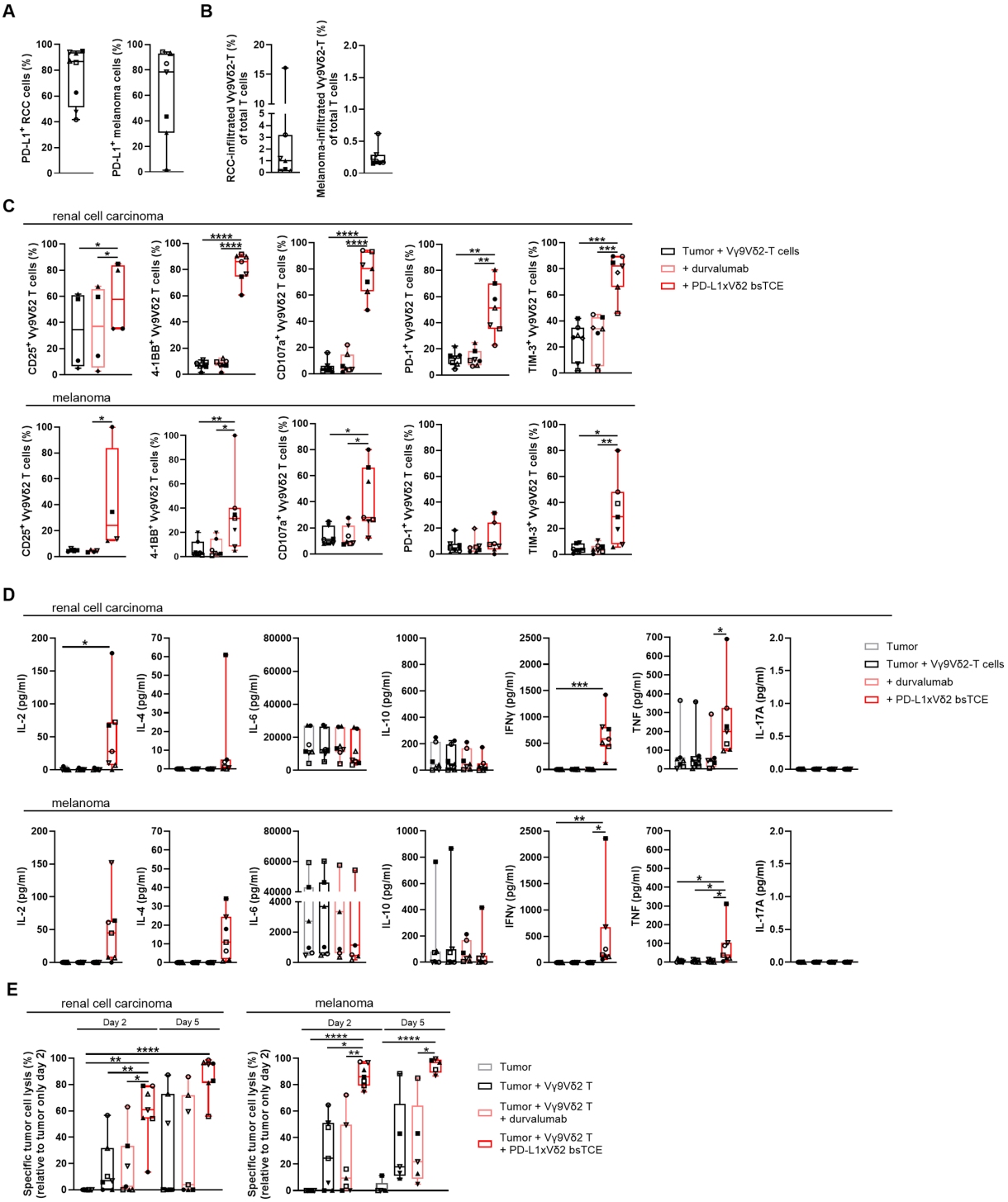

Figure 3 The PD-L1xVδ2 bsTCE triggers an antitumor immune response in RCC and melanoma single-cell suspensions. (A) Expression levels of PD-L1 (%) on RCC and melanoma-derived tumor cells (n=8) and (B) RCC-infiltrated and melanoma-infiltrated Vγ9Vδ2-T cell frequency of total CD3$^+$ T cells preculture. (C–E) Vγ9Vδ2-T cells were cultured for 2 or 5 days in a 1:10 E:T ratio with RCC or melanoma-derived single cell suspensions±durvalumab (10 µg/mL) or PD-L1xVδ2 bsTCE (100 nM). (C) Expression of CD25, 4-1BB, CD107a, PD-1 and TIM-3 on Vγ9Vδ2-T cells after 2 days of culture. (D) IL-2, IL-4, IL-6, IL-10, IFNγ and TNF levels detected in culture supernatant collected at day 2. (E) Lysis of tumor cells on day 2 and 5 relative to tumor condition day 2 (negative lysis=0%). Data are generated throughflow cytometry (A–C and E) or CBA (D). Individual data points are indicated using symbols and box and whisker plots indicate the median, 25th–75th percentiles and minimum to maximum. One-way ANOVA with Dunnett's multiple comparisons test was used (C–E), *p≤0.05, **p≤0.01, ***p≤0.001, ****p≤0.0001. ANOVA, analysis of variance; bsTCE, bispecific T cell engager; CBA, cytometric bead array; E:T, effector to target; IFNγ, interferon-gamma; IL, interleukin; PD-1, programmed death 1; PD-L1, programmed death ligand 1; RCC, renal cell carcinoma; TNF, tumor necrosis factor.

treated conditions, while levels of IL-6 and IL-10 did not notably change. In none of the conditions IL-17A could be detected. Lysis of the patient RCC and melanoma cells was assessed after 2 and 5 days of co-culture. Vγ9Vδ2-T cells alone exhibited variable tumor cytotoxicity against both RCC and melanoma cells, but this was significantly enhanced in the presence of the PD-L1xVδ2 bsTCE. The PD-L1xVδ2 bsTCE-induced tumor cell lysis increased between day 2 and day 5 (figure 3E). Durvalumab did not induce any Vγ9Vδ2-T cell activation nor enhance tumor cytotoxicity in these co-cultures.

Overall, these data showed that despite the presence of the (suppressive) TME, the PD-L1xVδ2 bsTCE could still trigger a robust Vγ9Vδ2-T cell-mediated antitumor response in tumor samples obtained from patients with RCC and metastatic melanoma.

PD-L1xVδ2 bsTCE-mediated Vγ9Vδ2-T cell engagement leads to coactivation of conventional $CD4^+$ and $CD8^+$ T cells and predominance of mature dendritic cells in the tumor microenvironment.

As it is known that interactions between PD-1 and PD-L1, expressed by tumor cells and tumor-infiltrating myeloid cells, drive effector T-cell dysfunction in the TME,[24] we next explored whether the PD-L1xVδ2 bsTCE could overcome such effects in tumor samples of patients with RCC and melanoma. For this purpose, dissociated RCC and melanoma samples were co-cultured for 48 hours with expanded Vγ9Vδ2-T cells at an E:T ratio of 1:10 in the presence or absence of either durvalumab or the PD-L1xVδ2 bsTCE. In the presence of the PD-L1xVδ2 bsTCE there was a statistically significant increase in the expression of the activation marker 4-1BB and the degranulation marker CD107a on both RCC infiltrating conventional $CD4^+$ and $CD8^+$ T cells (figure 4). A similar pattern was observed in melanoma tumor samples, though here it did not always reach statistical significance. With the exception of upregulation of CD25 on melanoma-infiltrating $CD8^+$ T cells and TIM-3 on RCC-infiltrating $CD8^+$ T cells, no other statistically significant changes were noted for CD25, PD-1 and TIM-3. While exposure of the tumor

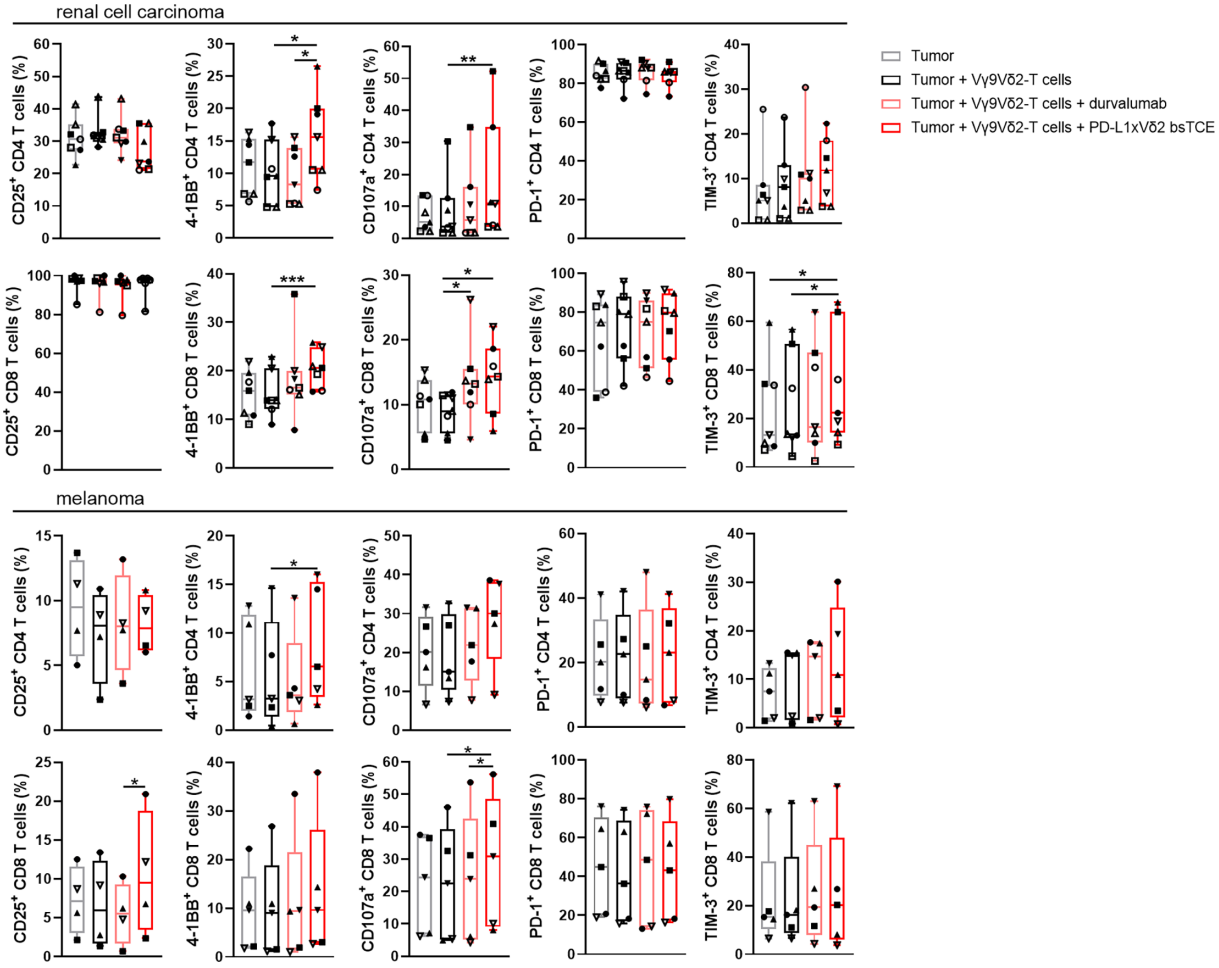

Figure 4 PD-L1xVδ2 bsTCE shapes an antitumor immune microenvironment with an increase in activated T cells. Vγ9Vδ2-T cells were cultured for 2 days in a 1:10 E:T ratio with RCC or melanoma-derived single cell suspensions±durvalumab (10 µg/mL) or PD-L1xVδ2 bsTCE (100 nM). Shown are expression levels of CD25, 4-1BB, CD107a, PD-1 and TIM-3 on tumor-infiltrated $CD4^+$ and $CD8^+$ T cells. Data are all generated throughflow cytometry. Individual data points are indicated using symbols and box and whisker plots indicate the median, 25th–75th percentiles and minimum to maximum. One-way ANOVA with Dunnett's multiple comparisons test was used, *p≤0.05, **p≤0.01. ANOVA, analysis of variance; bsTCE, bispecific T cell engager; E:T, effector to target; PD-1, programmed death 1; PD-L1, programmed death ligand 1; RCC, renal cell carcinoma.

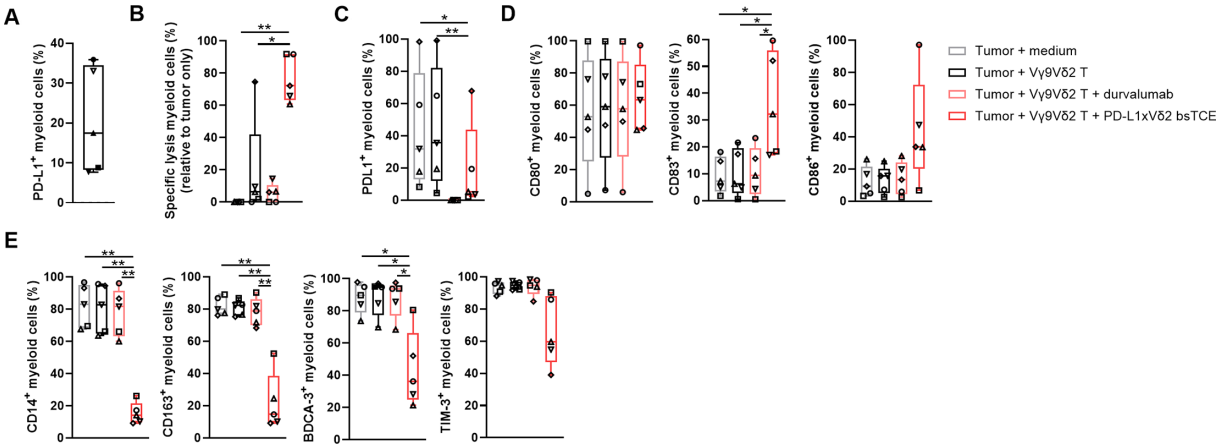

Figure 5 PD-L1xVδ2 bsTCE shapes an antitumor immune microenvironment with mature dendritic cell-like myeloid cells. Vγ9Vδ2-T cells were cultured for 5 days in a 1:10 E:T ratio with melanoma-derived single cell suspensions±durvalumab (10 µg/mL) or PD-L1xVδ2 bsTCE (100 nM). (A) Expression levels of PD-L1 (%) on CD45$^+$HLA$^-$DR$^+$CD11c$^+$ myeloid cells (n=5) preculture. (B) Lysis of myeloid cells relative to tumor+medium condition (negative lysis=0%) postculture. (C) Expression levels of PD-L1 on myeloid cells postculture. (D) Expression levels of CD80, CD83 and CD86 on myeloid cells. (E) Expression levels of CD14, CD163, BDCA-3 and TIM-3 on myeloid cells. Data are all generated throughflow cytometry. Individual data points are indicated using symbols and box and whisker plots indicate the median, 25th–75th percentiles and minimum to maximum. One-way ANOVA with Dunnett's multiple comparisons test was used, *p≤0.05, **p≤0.01. ANOVA, analysis of variance; bsTCE, bispecific T cell engager; E:T, effector to target; PD-L1, programmed death ligand 1.

samples to durvalumab in some cases resulted in minor (not statistically significant) differences in marker expression, the modulatory effects triggered by the presence of the PD-L1xVδ2 bsTCE were clearly more pronounced and suggestive of a direct contribution of the activated Vγ9Vδ2-T cells over inhibition of the PD-1/PD-L1 checkpoint alone.

We next assessed whether the PD-L1xVδ2 bsTCE could affect the frequency and phenotype of myeloid cells. For this purpose, melanoma patient-derived single-cell tumor suspensions were cultured with expanded Vγ9Vδ2-T cells (E:T ratio 1:10) in the presence or absence of durvalumab or the PD-L1xVδ2 bsTCE for 5 days. At baseline, PD-L1 was found to be expressed by a median of 17.5% (range 7.7–35.9%, figure 5A) of the myeloid cells (defined as CD45$^+$HLA-DR$^+$CD11c^{high}) and gated to exclude lymphocytes[25]. As these cultures were performed from cryopreserved samples, no surviving granulocytes were present in the cultures and we have previously shown that all thus gated myeloid cells are from monocytic origins based on CD88 and CD89 expression.[25] on co-culture with Vγ9Vδ2-T cells, the PD-L1xVδ2 bsTCE triggered substantial lysis of myeloid cells (figure 5B). The observed lysis typically exceeded the percentage of myeloid cells expressing PD-L1 at baseline, which may be due to upregulation of PD-L1 during the co-culture (ie, by IFNγ produced by activated Vγ9Vδ2-T cells).[23] Indeed, myeloid cell PD-L1 was typically increased at day 5, except in the conditions exposed to durvalumab (where reliable PD-L1 assessment was complicated by interference with the mAb used for PD-L1 detection) and the PD-L1xVδ2 bsTCE, likely because of lysis of the PD-L1 expressing myeloid cells (figure 5C). Of interest, in the cultures exposed to the PD-L1xVδ2 bsTCE, a clear phenotypic shift could be noted in the remaining myeloid cells. While CD80 expression remained unchanged, expression of CD83 and CD86 was significantly increased on these cells, indicative of a phenotype consistent with mature dendritic cells (figure 5D). These cells also exhibited significantly reduced expression of CD14, CD163 and BDCA-3, along with a trend towards lower TIM-3 levels, suggesting a phenotype associated with attenuated suppressive and enhanced T-cell stimulatory functionality (figure 5E).

Overall, these data demonstrate that the PD-L1xVδ2 bsTCE can trigger Vγ9Vδ2-T cells to mediate a shift in the TME characterized by an increase in 4-1BB and CD107a expressing CD4$^+$ and CD8$^+$ T cells, elimination of PD-L1 expressing tumor and myeloid cells and an associated increase in rates of mature dendritic cells expressing higher levels of co-stimulatory molecules and lower levels of suppression related receptors.

PD-L1xVδ2 bsTCE engaged Vγ9Vδ2-T cells infiltrate tumor cell-derived spheroids and trigger their lysis

Tumor spheroids were generated and used as a model to determine PD-L1xVδ2 bsTCE-mediated infiltration and cytolytic effects of Vγ9Vδ2-T cells in a three-dimensional tumor model (illustrated in figure 6A). Spheroids were generated by culturing melanoma-derived BRO tumor cells overnight in non-adhesive culture plates. During this overnight incubation, BRO tumor cells retained PD-L1 expression (figure 6B). Spheroids were subsequently co-cultured with expanded Vγ9Vδ2-T cells for an additional 8 hours, during which confocal microscopy in combination with Z-stacks (stack of images captured at different focal depths along the Z-axis) was used to image and track Vγ9Vδ2-T cells, or 24 hours after which the supernatant, containing non-infiltrated Vγ9Vδ2-T

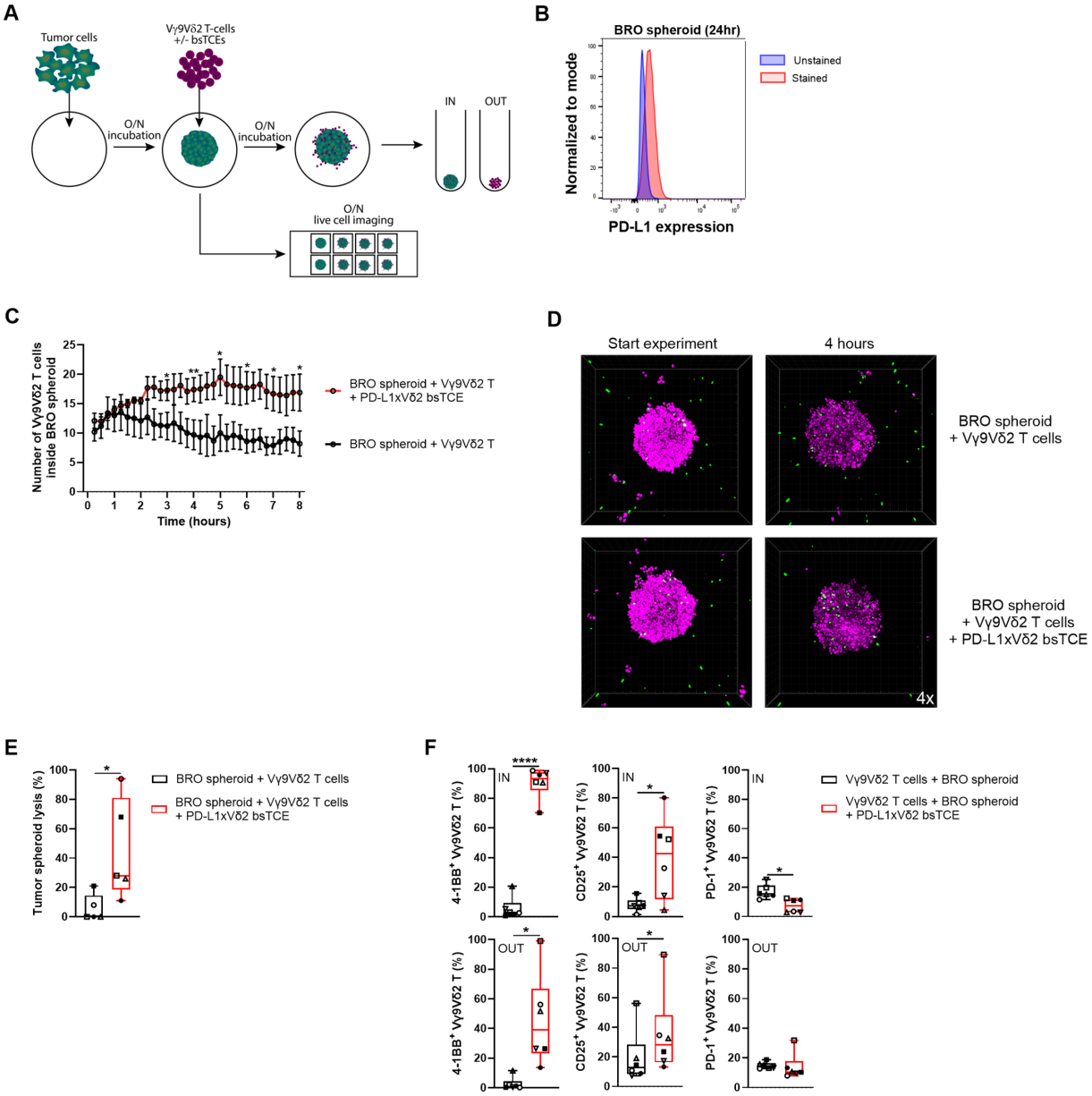

Figure 6 PD-L1xVδ2 bsTCE induces Vγ9Vδ2-T cell infiltration into BRO spheroid, tumor lysis and activation of infiltrated Vγ9Vδ2-T cells. (A) Illustration of tumor spheroid formation and functional assays. (B) PD-L1 expression levels on BRO spheroid after O/N culture shown in histogram (n=1). (C–D) Vγ9Vδ2-T cell infiltration into BRO tumor spheroids over time (8 hours)±100 nM PD-L1xVδ2 bsTCE (C, n=5). (D) Representative slides of a Z-stack of 1 Vγ9Vδ2-T cell donor is shown at a 4× enlargement at the start of the experiment and 4 hours later (green=Vγ9Vδ2-T cells and purple=BRO tumor cells). (E–F) Lysis of BRO spheroids and expression of 4-1BB, CD25 and PD-1 (%) on infiltrated (IN) and non-infiltrated (OUT) Vγ9Vδ2-T cells (E, n=6) and (F, n=5) after 24 hours co-culture±100 nM PD-L1xVδ2 bsTCE. C: data is generated through confocal microscopy, shown are mean±SEM and paired t-test was used. D: data is generated through confocal microscopy and images were made using Imaris software. E–F: data are generated throughflow cytometry, individual data points are indicated using symbols and box and whisker plots indicate the median, 25th–75th percentiles and minimum to maximum and one-way ANOVA with Dunnett's multiple comparisons test was used. *p≤0.05, **p≤0.01, ****p≤0.0001. ANOVA, analysis of variance; bsTCE, bispecific T cell engager; PD-1, programmed death 1; PD-L1, programmed death ligand 1.

cells (termed OUT), was harvested and these OUT Vγ9Vδ2-T cells were compared with infiltrated Vγ9Vδ2-T cells retrieved from the spheroids after trypsinization (termed IN). The PD-L1xVδ2 bsTCE promoted rapid infiltration of Vγ9Vδ2-T cells into BRO spheroids within the first 2–3 hours, after which it stabilized (figure 6C). In the absence of the PD-L1xVδ2 bsTCE, some Vγ9Vδ2-T cell infiltration was observed in the first hour, but decreased thereafter. As depicted in figure 6D, in the absence of the PD-L1xVδ2 bsTCE, Vγ9Vδ2-T cells (green) predominantly surrounded the BRO spheroid (purple) without showing substantial infiltration. In the presence of the PD-L1xVδ2 bsTCE, clear infiltration of the Vγ9Vδ2-T cells into the spheroid was noted. As expected, Vγ9Vδ2-T cells

cultured in the presence of the PD-L1xVδ2 bsTCE triggered variable, but statistically significant, lysis of BRO spheroid tumor cells during the 24 hours co-culture (figure 6E). Lysis was highest in the donors that exhibited higher baseline tumor reactivity, possibly related to differences in BTN2A1/3A1, NKG2D and DNAM-1 interactions between Vγ9Vδ2-T cell donors. Co-cultures that were performed in the presence of the PD-L1xVδ2 bsTCE resulted in significant upregulation of the activation markers 4-1BB and CD25 on both spheroid-infiltrated and non-infiltrated Vγ9Vδ2-T cells (figure 6F). In contrast, PD-1 expression levels on Vγ9Vδ2-T cells that had infiltrated the spheroids were actually significantly lower than in the medium control while they were similar on the Vγ9Vδ2-T cells that had not infiltrated the spheroids. Interestingly, in the presence of the PD-L1xVδ2 bsTCE, infiltrated Vγ9Vδ2-T cells expressed significantly higher levels of 4-1BB (p=0.017) and a trend towards lower levels of PD-1 (p=0.067) compared with non-infiltrated Vγ9Vδ2-T cells that were also exposed to the PD-L1xVδ2 bsTCE. No differences were observed for CD25 levels between infiltrated and non-infiltrated Vγ9Vδ2-T cells (p=0.781) exposed to the PD-L1xVδ2 bsTCE.

Collectively, these findings demonstrate that the PD-L1xVδ2 bsTCE enhances Vγ9Vδ2-T cell infiltration into tumor spheroids, leading to their lysis. Within these spheroids, Vγ9Vδ2-T cells exhibit elevated expression of activation markers 4-1BB and CD25, alongside low expression of the checkpoint inhibitor PD-1, suggesting reduced sensitivity to inhibitory signaling.

DISCUSSION

Approved PD-1/PD-L1 immune checkpoint inhibitors can exhibit significant antitumor activity in patients with various solid tumors including melanoma and RCC.[1 3] Nevertheless, efficacy is typically confined to a smaller subset of patients and frequently not long-lasting and hence there is a need to enhance current therapeutic strategies and explore novel approaches to allow for broader patient benefit. Here, we generated a bsTCE targeting PD-L1 and Vγ9Vδ2-T cells with triple functionality: (re)-activation of conventional T cells via PD-1/PD-L1 immune checkpoint blockade and redirection of Vγ9Vδ2-T cells towards PD-L1$^+$ tumor cells and PD-L1$^+$ myeloid cells resulting in their lysis and modulation of the TME.

In order to endow the PD-L1xVδ2 bsTCE with the PD-1/PD-L1 immune checkpoint inhibition ability, we first compared a set of PD-L1 specific VHHs for their ability to interfere with PD-1 binding to PD-L1 and to functionally release PD-1 expressing cells from the inhibitory effect mediated through PD-L1. The selected PD-L1 specific VHH was then fused to a Vδ2-TCR specific VHH, resulting in a PD-L1xVδ2 bsTCE that exhibited high (sub nM) affinity to both PD-L1 and Vγ9Vδ2-T cells and that triggered strong activation and degranulation of Vγ9Vδ2-T cells and the effective lysis of PD-L1 transfected tumor cells and PD-L1 expressing cancer patient-derived tumor cell lines. These data align with our prior findings exploring the use of Vδ2-bsTCEs targeting other TAAs.[6–10] Of interest, the PD-L1xVδ2 bsTCE also triggered lysis of melanoma cell lines that expressed relatively low basal PD-L1 levels. Although speculative, this may be explained by further upregulation of PD-L1 expression on tumor cells in response to IFNγ,[23] a proinflammatory cytokine produced by activated Vγ9Vδ2-T cells on engagement by Vδ2-bsTCEs.[9 10] Indeed, when we exposed the melanoma cell lines and patient tumor cells to IFNγ, PD-L1 expression levels increased rendering the cells theoretically more susceptible to PD-L1xVδ2 bsTCE-mediated effects. This effect may be further facilitated by the inherent tumor sensing ability of Vγ9Vδ2-T cells.[26 27]

When exploring the effect of the PD-L1xVδ2 bsTCE in co-cultures of Vγ9Vδ2-T cells and patient-derived metastatic melanoma and RCC single-cell suspensions, that is, samples that included cells of the tumor microenvironment, we not only observed the expected activation of Vγ9Vδ2-T cells, but also an upregulation of the expression of the activation marker 4-1BB and the degranulation marker CD107a on tumor-infiltrating CD4$^+$ and CD8$^+$ T cells. Supernatants from these cultures contained elevated levels of proinflammatory cytokines IFNγ and TNF, likely produced by activated Vγ9Vδ2-T cells and conventional T cells. As no such effects were observed in the presence of durvalumab, the PD-L1xVδ2 bsTCE-induced effects are likely secondary to and dominated by Vγ9Vδ2-T cell activation rather than just PD-1/PD-L1 immune checkpoint blockade. The activation of conventional CD4$^+$ and CD8$^+$ T cells in our ex vivo cultures could be driven by direct antigen presentation by bsTCE-activated Vγ9Vδ2-T cells,[10] the observed reduction of immunosuppressive myeloid cells, which are known to inhibit T cell activation,[28] and/or the release of pro-inflammatory cytokines by bsTCE-activated Vγ9Vδ2-T cells.[9] The relative contribution of each of these mechanisms to the observed αβ-T cell activation remains unclear.

Literature reports that the costimulatory signal via CD28/B7 interactions remains critical for optimal restoration of T cell effector function under PD-1/PD-L1 blockade.[29] CD28 has been shown to be required for PD-1 inhibition to be effective and points to the need for CD80/CD86 costimulation in addition to disrupting PD-1 binding to PD-L1 alone.[29 30] In line with this, proliferative CD8$^+$ T cells were found on clinical PD-1 blockade which were located in close proximity with conventional DCs, which can provide CD80/CD86 costimulation.[31–33] Similarly, Garris and colleagues showed that robust activation of antitumor T cells by anti-PD-1 therapy required T-cell-DC interactions and was facilitated by IFNγ and IL-12.[34] In our experiments with patient-derived metastatic melanoma single-cell suspensions, we not only observed a reduction of tumor cells, but also a notable reduction in the number of PD-L1$^+$ myeloid cells on exposure to the PD-L1xVδ2 bsTCE, indicating that both PD-L1-expressing cell populations can contribute to

the activation of Vγ9Vδ2-T cells within ex vivo cultures. Of note, the remaining myeloid cells expressed higher levels of CD83 and CD86, which is indicative of a shift in the myeloid cell compartment towards a more mature dendritic cell population with costimulatory potential,[35 36] which is essential for T cell activation.[37 38] As this myeloid cell population also showed reduced expression of suppression-related markers like PD-L1, CD14, CD163, BDCA-3 and TIM-3,[39] these data are suggestive of a beneficial immunomodulatory effect of the PD-L1xVδ2 bsTCE in the TME. The observed shift towards more mature dendritic cells could be the result of lysis of specifically immature myeloid cells expressing high levels of PD-L1, CD14, CD163, BDCA-3 and TIM-3, and/or differentiation of myeloid cells towards mature dendritic cells due to proinflammatory cytokine release by bsTCE-activated Vγ9Vδ2-T cells. As these mature dendritic cells express PD-L1, yet remain viable in culture, it is possible they use the SerpinB9 protease inhibitor to inactivate granzyme B and thereby avoid lysis by activated Vγ9Vδ2-T cells.[40] The overall relevance of the observed changes is underscored by the observation that a reduction in myeloid cells, particularly myeloid-derived suppressor cells, in patients treated with anti-PD-1 mAbs has been linked to disease control.[41]

A key factor contributing to resistance to immune checkpoint blockade is related to the insufficient presence or infiltration of T cells into the tumor microenvironment.[42] In experiments where we used three-dimensional tumor spheroids of melanoma, the PD-L1xVδ2 bsTCE resulted in a clear enhancement of tumor infiltration by Vγ9Vδ2-T cells. This was accompanied by robust activation of the infiltrated Vγ9Vδ2-T cells and lysis of the tumor cells. The enhanced infiltration of Vγ9Vδ2-T cells could possibly be secondary to the bsTCE-mediated synapse formation which allows Vγ9Vδ2-T cells to attach to the spheroid and facilitate infiltration. Our previous findings demonstrated that bsTCE-activated Vγ9Vδ2-T cells produce the leukocyte-attracting chemokines CCL5, CXCL10 and CXCL11,[9] which may contribute to the enhanced migratory capacity and infiltration observed in the present study. In addition to the inflammatory environment that the PD-L1xVδ2 bsTCE can create through both enhancement of infiltration and activation of Vγ9Vδ2-T cells into the tumor and the noted shift in the myeloid compartment, activated Vγ9Vδ2 T cells (including Vδ2 bsTCE activated Vγ9Vδ2-T cells) have also been shown to act as APCs with the ability to (cross-) present antigens to both $CD4^+$ and $CD8^+$ T cells.[13 43 44] This can potentially further drive the development of a broader, more effective antitumor response involving mobilization of conventional T cells to the tumor site.

In conclusion, the PD-L1xVδ2 bsTCE that we generated allows for a multimodal approach to cancer immunotherapy by acting as a PD-1/PD-L1 immune checkpoint inhibitor, by enhancing Vγ9Vδ2-T cell activation, infiltration and tumor lysis, and by reshaping the tumor microenvironment into a more proinflammatory state. By targeting both PD-L1-expressing tumor and myeloid cells, while activating conventional effector T cells and dendritic cells, it addresses key challenges of current therapies, and thereby offers a promising novel therapeutic strategy.

Author affiliations
[1]Department of Medical Oncology, Amsterdam UMC, Vrije Universiteit Amsterdam, Amsterdam, The Netherlands
[2]Cancer Centre Amsterdam, Amsterdam, The Netherlands
[3]Amsterdam Institute for Infection and Immunity, Amsterdam, The Netherlands
[4]Department of Molecular Cell Biology and Immunology, Amsterdam UMC, Vrije Universiteit Amsterdam, Amsterdam, The Netherlands
[5]Lava Therapeutics NV, Utrecht, The Netherlands

Acknowledgements We thank all the patients who agreed to donate samples for this study and Tereza Brachtlová for generating the melanoma cell lines MEL-23 and MEL-25.

Contributors LAK, HJvdV, and TDdG contributed to conception and design of the study. LAK, MV, MR, GLS and MAP performed experiments. LAK, MV and GLS performed experimental analysis and interpreted the results. HJvdV and TDdG provided supervision. LAK wrote the first draft of the manuscript. HJvdV and TDdG reviewed and revised the manuscript. All authors read and approved the submitted version. LAK is the guarantor.

Funding The research was funded by Lava Therapeutics NV, Utrecht, The Netherlands. LAVA Therapeutics employees were involved in the design of the study and interpretation of data. LAVA Therapeutics approved the manuscript before submission.

Competing interests HJvdV and TDdG hold stock from Lava Therapeutics. HJvdV is employed by Lava Therapeutics and received research funding (to employ LAK and MV) from Lava Therapeutics. TDdG is scientific advisor to Lava Therapeutics. All other authors declare that the research was conducted in the absence of any commercial or financial relationships that could be construed as a potential conflict of interest.

Patient consent for publication Not applicable.

Ethics approval Patients were enrolled under written informed consent in an institutional review board (IRB)-approved clinical study of autologous whole-cell vaccination at the Amsterdam UMC, location VUmc (Amsterdam, The Netherlands, reference number 2003-37).[20 45]

Provenance and peer review Not commissioned; externally peer reviewed.

Data availability statement Data are available upon reasonable request.

ORCID iD
Lisa A King https://orcid.org/0009-0001-8705-150X

REFERENCES

1 Postow MA, Callahan MK, Wolchok JD. Immune Checkpoint Blockade in Cancer Therapy. *J Clin Oncol* 2015;33:1974–82.

2 Freeman GJ, Long AJ, Iwai Y, *et al*. Engagement of the PD-1 immunoinhibitory receptor by a novel B7 family member leads to negative regulation of lymphocyte activation. *J Exp Med* 2000;192:1027–34.
3 Schumacher TN, Schreiber RD. Neoantigens in cancer immunotherapy. *Science* 2015;348:69–74.
4 Nowicki TS, Hu-Lieskovan S, Ribas A. Mechanisms of Resistance to PD-1 and PD-L1 Blockade. *Cancer J* 2018;24:47–53.
5 Sharma P, Hu-Lieskovan S, Wargo JA, *et al*. Primary, Adaptive, and Acquired Resistance to Cancer Immunotherapy. *Cell* 2017;168:707–23.
6 de Weerdt I, Lameris R, Ruben JM, *et al*. A Bispecific Single-Domain Antibody Boosts Autologous Vγ9Vδ2-T Cell Responses Toward CD1d in Chronic Lymphocytic Leukemia. *Clin Cancer Res* 2021;27:1744–55.
7 de Weerdt I, Lameris R, Scheffer GL, *et al*. A Bispecific Antibody Antagonizes Prosurvival CD40 Signaling and Promotes Vγ9Vδ2 T cell-Mediated Antitumor Responses in Human B-cell Malignancies. *Cancer Immunol Res* 2021;9:50–61.
8 Lameris R, Ruben JM, Iglesias-Guimarais V, *et al*. A bispecific T cell engager recruits both type 1 NKT and Vγ9Vδ2-T cells for the treatment of CD1d-expressing hematological malignancies. *Cell Rep Med* 2023;4:100961.
9 King LA, Toffoli EC, Veth M, *et al*. A Bispecific γδ T-cell Engager Targeting EGFR Activates a Potent Vγ9Vδ2 T cell-Mediated Immune Response against EGFR-Expressing Tumors. *Cancer Immunol Res* 2023;11:1237–52.
10 King LA, Veth M, Iglesias-Guimarais V, *et al*. Leveraging Vγ9Vδ2 T cells against prostate cancer through a VHH-based PSMA-Vδ2 bispecific T cell engager. *iScience* 2024;27:111289.
11 Harly C, Guillaume Y, Nedellec S, *et al*. Key implication of CD277/butyrophilin-3 (BTN3A) in cellular stress sensing by a major human γδ T-cell subset. *Blood* 2012;120:2269–79.
12 Rigau M, Ostrouska S, Fulford TS, *et al*. Butyrophilin 2A1 is essential for phosphoantigen reactivity by γδ T cells. *Science* 2020;367:eaay5516.
13 Brandes M, Willimann K, Moser B. Professional antigen-presentation function by human gammadelta T Cells. *Science* 2005;309:264–8.
14 Saura-Esteller J, de Jong M, King LA, *et al*. Gamma Delta T-Cell Based Cancer Immunotherapy: Past-Present-Future. *Front Immunol* 2022;13:915837.
15 Paniagua-Herranz L, Díaz-Tejeiro C, Sanvicente A, *et al*. Overcoming limitations for antibody-based therapies targeting γδ T (Vg9Vd2) cells. *Front Immunol* 2024;15:1432015.
16 de Bruin RCG, Lougheed SM, van der Kruk L, *et al*. Highly specific and potently activating Vγ9Vδ2-T cell specific nanobodies for diagnostic and therapeutic applications. *Clin Immunol* 2016;169:128–38.
17 Lockshin A, Giovanella BC, De Ipolyi PD, *et al*. Exceptional lethality for nude mice of cells derived from a primary human melanoma. *Cancer Res* 1985;45:345–50.
18 Karasic TB, Hei TK, Ivanov VN. Disruption of IGF-1R signaling increases TRAIL-induced apoptosis: a new potential therapy for the treatment of melanoma. *Exp Cell Res* 2010;316:1994–2007.
19 Jorritsma A, Gomez-Eerland R, Dokter M, *et al*. Selecting highly affine and well-expressed TCRs for gene therapy of melanoma. *Blood* 2007;110:3564–72.
20 Baars A, Claessen AM, van den Eertwegh AJ, *et al*. Skin tests predict survival after autologous tumor cell vaccination in metastatic melanoma: experience in 81 patients. *Ann Oncol* 2000;11:965–70.
21 Vermorken JB, Claessen AM, van Tinteren H, *et al*. Active specific immunotherapy for stage II and stage III human colon cancer: a randomised trial. *Lancet* 1999;353:345–50.
22 Kohabir KAV, Linthorst J, Nooi LO, *et al*. Synthetic mismatches enable specific CRISPR-Cas12a-based detection of genome-wide SNVs tracked by ARTEMIS. *Cell Rep Methods* 2024;4:100912.
23 Garcia-Diaz A, Shin DS, Moreno BH, *et al*. Interferon Receptor Signaling Pathways Regulating PD-L1 and PD-L2 Expression. *Cell Rep* 2019;29:3766.
24 Jiang T, Bai Y, Zhou F, *et al*. Clinical value of neutrophil-to-lymphocyte ratio in patients with non-small-cell lung cancer treated with PD-1/PD-L1 inhibitors. *Lung Cancer (Auckl)* 2019;130:76–83.
25 Dudziak D, Heger L, Agace WW, *et al*. Guidelines for preparation and flow cytometry analysis of human nonlymphoid tissue DC. *Eur J Immunol* 2025;55:2250325.
26 Corvaisier M, Moreau-Aubry A, Diez E, *et al*. V gamma 9V delta 2 T cell response to colon carcinoma cells. *J Immunol* 2005;175:5481–8.
27 Bouet-Toussaint F, Cabillic F, Toutirais O, *et al*. Vgamma9Vdelta2 T cell-mediated recognition of human solid tumors. Potential for immunotherapy of hepatocellular and colorectal carcinomas. *Cancer Immunol Immunother* 2008;57:531–9.
28 Srivastava MK, Sinha P, Clements VK, *et al*. Myeloid-derived suppressor cells inhibit T-cell activation by depleting cystine and cysteine. *Cancer Res* 2010;70:68–77.
29 Kamphorst AO, Wieland A, Nasti T, *et al*. Rescue of exhausted CD8 T cells by PD-1-targeted therapies is CD28-dependent. *Science* 2017;355:1423–7.
30 Hui E, Cheung J, Zhu J, *et al*. T cell costimulatory receptor CD28 is a primary target for PD-1-mediated inhibition. *Science* 2017;355:1428–33.
31 Jansen CS, Prokhnevska N, Master VA, *et al*. An intra-tumoral niche maintains and differentiates stem-like CD8 T cells. *Nature New Biol* 2019;576:465–70.
32 Tumeh PC, Harview CL, Yearley JH, *et al*. PD-1 blockade induces responses by inhibiting adaptive immune resistance. *Nature New Biol* 2014;515:568–71.
33 Sade-Feldman M, Yizhak K, Bjorgaard SL, *et al*. Defining T Cell States Associated with Response to Checkpoint Immunotherapy in Melanoma. *Cell* 2018;175:998–1013.
34 Garris CS, Arlauckas SP, Kohler RH, *et al*. Successful Anti-PD-1 Cancer Immunotherapy Requires T Cell-Dendritic Cell Crosstalk Involving the Cytokines IFN-γ and IL-12. *Immunity* 2018;49:1148–61.
35 Dilioglou S, Cruse JM, Lewis RE. Function of CD80 and CD86 on monocyte- and stem cell-derived dendritic cells. *Exp Mol Pathol* 2003;75:217–27.
36 Prechtel AT, Steinkasserer A. CD83: an update on functions and prospects of the maturation marker of dendritic cells. *Arch Dermatol Res* 2007;299:59–69.
37 Bernard NJ. Co-stimulation needed in the tumor. *Nat Immunol* 2023;24:204.
38 Kleinovink JW, Marijt KA, Schoonderwoerd MJA, *et al*. PD-L1 expression on malignant cells is no prerequisite for checkpoint therapy. *Oncoimmunology* 2017;6:e1294299.
39 van de Ven R, Lindenberg JJ, Oosterhoff D, *et al*. Dendritic Cell Plasticity in Tumor-Conditioned Skin: CD14(+) Cells at the Cross-Roads of Immune Activation and Suppression. *Front Immunol* 2013;4:403.
40 Medema JP, Schuurhuis DH, Rea D, *et al*. Expression of the serpin serine protease inhibitor 6 protects dendritic cells from cytotoxic T lymphocyte-induced apoptosis: differential modulation by T helper type 1 and type 2 cells. *J Exp Med* 2001;194:657–67.
41 Limagne E, Richard C, Thibaudin M, *et al*. Tim-3/galectin-9 pathway and mMDSC control primary and secondary resistances to PD-1 blockade in lung cancer patients. *Oncoimmunology* 2019;8:e1564505.
42 Wang MM, Coupland SE, Aittokallio T, *et al*. Resistance to immune checkpoint therapies by tumour-induced T-cell desertification and exclusion: key mechanisms, prognostication and new therapeutic opportunities. *Br J Cancer* 2023;129:1212–24.
43 Brandes M, Willimann K, Bioley G, *et al*. Cross-presenting human gammadelta T cells induce robust CD8+ alphabeta T cell responses. *Proc Natl Acad Sci U S A* 2009;106:2307–12.
44 Meuter S, Eberl M, Moser B. Prolonged antigen survival and cytosolic export in cross-presenting human gammadelta T cells. *Proc Natl Acad Sci U S A* 2010;107:8730–5.
45 Koster BD, Santegoets SJAM, Harting J, *et al*. Autologous tumor cell vaccination combined with systemic CpG-B and IFN-α promotes immune activation and induces clinical responses in patients with metastatic renal cell carcinoma: a phase II trial. *Cancer Immunol Immunother* 2019;68:1025–35.